Aerospace Science and Technology 84 (2019) 895–903

Contents lists available at ScienceDirect

Aerospace Science and Technology

www.elsevier.com/locate/aescte

Smooth-switching LPV control for vibration suppression of a flexible airplane wing

Tianyi He [a], Guoming G. Zhu [a,*], Sean S.-M. Swei [b], Weihua Su [c]

[a] Department of Mechanical Engineering, Michigan State University, East Lansing, MI, 48823, United States of America
[b] Intelligent Systems Division, NASA Ames Research Center, Moffett Field, CA, 94035, United States of America
[c] Department of Aerospace Engineering and Mechanics, University of Alabama, Tuscaloosa, AL, 35487, United States of America

ARTICLE INFO

Article history:
Received 26 September 2018
Received in revised form 15 November 2018
Accepted 16 November 2018
Available online 22 November 2018

ABSTRACT

In this paper, active vibration suppression of a Blended-Wing-Body flexible airplane wing is studied by utilizing a smooth-switching linear parameter-varying (LPV) dynamic output-feedback control. For the reduced-order LPV models, developed for each divided flight envelop subregion, a family of mixed Input Covariance Constraint and $\mathcal{H}_\infty$ LPV controllers are designed to robustly suppress the wing bending displacement using hard-constrained control surfaces, while achieving smooth-switching between adjacent controllers. The proposed LPV controllers are developed by minimizing a combination of weighted $\mathcal{H}_2$ output performance and smoothness index, subject to a set of Parametric Linear Matrix Inequalities derived from stability and performance conditions. In addition, the weighting coefficient in the cost function is tuned to balance between $\mathcal{H}_2$ performance and switching smoothness by iteratively solving convex optimization problems. Simulation results demonstrate that simultaneous smooth-switching and improved performance can be achieved by the proposed LPV control.

1. Introduction

With the advantages of high aerodynamic and fuel efficiency, light and flexible airplane wing design is considered as a promising candidate for next-generation commercial aircraft as well as emerging air vehicle concept. However, vehicle flexibility often results in strong coupling between structural modes and rigid body dynamics, which poses a great challenge for modeling and flight control. In our previous work, a systematic framework of linear parameter-varying (LPV) modeling and control for active vibration suppression has been proposed and applied to a Blended-Wing-Body (BWB) flexible airplane wing [1,2]. The LPV model is able to capture the variations of coupled modes at different flight speeds and depicts varying input–output relationship between flap deflection angles (control surfaces) and wing bending displacements (controlled outputs). A mixed Input Covariance Constraint (ICC [3]) and $\mathcal{H}_\infty$ state-feedback LPV control technique [4] was used to suppress bending displacements of the flexible wing by adapting flap deflection angles, where control input constraints are handled by ICC constraints and the modeling errors are dealt with by $\mathcal{H}_\infty$ constraints. Non-switching LPV state-feedback control was utilized in the previous study [5], and this paper extends to the smooth-switching LPV dynamic output-feedback (DOF) control to reduce the design conservativeness and make the LPV control practical with DOF control. Note that two significant contributions are made and they are the smooth-switching LPV control and extending the state feedback control to DOF control.

The current LPV modeling framework is often established in modal coordinates, hence for practical feedback implementation, the modal states need to be mapped back from their modal coordinates to the original physical coordinates. Accessing mapped states for state-feedback design is complex and requires extensive computational effort. However, these can be avoided in DOF control framework. Moreover, in practice the output measurements (bending displacements) are much easier to access with available sensors.

Switching LPV control utilizing multiple parameter-dependent Lyapunov functions (PDLFs) [6] was proposed to reduce conservativeness, leading to improved closed-loop performance when compared to the non-switching LPV control derived from a single Lyapunov function. Given partitioned subregions of scheduling parameters, multiple PDLFs are utilized to derive a family of Parametric Linear Matrix Inequalities (PLMIs) based on specific performance criteria and switching stability conditions. Gain-scheduling controllers are determined by minimizing the convex objective function subject to these formulated PLMIs over all subregions

* Corresponding author.
E-mail addresses: hetiany2@egr.msu.edu (T. He), zhug@egr.msu.edu (G.G. Zhu), sean.s.swei@nasa.gov (S.S.-M. Swei), suw@eng.ua.edu (W. Su).

https://doi.org/10.1016/j.ast.2018.11.029
1270-9638/

simultaneously. Many engineering applications of switching LPV control have demonstrated system performance improvement over non-switching LPV control [6–9] due to reduced design conservativeness. However, an abrupt change in control and response over the switching surface can be observed, and this un-smooth transient response can be attributed to abrupt changes in controller gains during switching. This is because the closed-loop system performance is optimized at each subregion during conventional control design, and the smooth transition between adjacent controllers are not considered. The extrema-seeking system performance at each subregion without considering switching performance often leads to high-gain controllers, hence resulting in an un-smooth switching between these high-gain controllers. This can be easily validated by examining the control gain differences between two neighboring subregions over the switching surface.

In literature, only a few publications are available in addressing ways to reduce the abrupt jumps, and the smooth-switching LPV control design is still considered an open problem. Chen [10] considered the hysteresis switching state-feedback LPV control and conducted linear interpolation of controller variables on switching surfaces to achieve smooth-switching during switch-in and switch-out on the overlapping region. However, this method cannot quantitatively evaluate switching smoothness and only a relative stability is achieved on the overlapping subregion. Hanifzadegan and Nagamune [11] followed the idea of linear interpolation of controller matrices on switching surfaces, introduced a measure of smoothness index and imposed constraints on controller matrix derivative to compensate for the drawbacks found in Chen [10]. The design of stabilizing controllers was formulated into a non-convex optimization problem, and an iterative descent algorithm was then applied to find local LPV controller for each individual subregion. Their approach relies heavily on iterative computations to solve multi-objective non-convex problems. Moreover, the introduced smoothness index lacks physical meaning and the smoothness constraints on controller matrices and their rates are selected through trial and error. In addition, the interpolation of controller matrices cannot guarantee the $\mathcal{H}_\infty$ robust performance on the overlapped region.

In this paper, a convex optimization problem is formulated to simultaneously design smooth-switching LPV DOF controllers over divided subregions. Instead of using linear interpolation, a numerically tractable smoothness index is introduced in the optimization cost function. Here the smoothness index is defined by taking the normed difference of controller variable matrices between any two switching surfaces. By means of minimizing this smoothness index, it can be demonstrated that sharp changes in states and outputs can be significantly reduced at the cost of degraded system performance. In other words, there exists a trade-off relationship between system performance and switching smoothness, and hence a tunable weighting parameter is adopted in the cost function. By tuning the weighting parameter, an optimal trade-off can be reached, leading to a smooth-switching LPV controller with acceptable system performance.

A smooth-switching mixed ICC/$\mathcal{H}_\infty$ LPV control is developed in this study and applied to active vibration suppression of a BWB flexible airplane wing, and is able to demonstrate improved $\mathcal{H}_2$ performance with guaranteed $\mathcal{H}_\infty$ robust performance and subject to ICC hard-constrains on control inputs. The main contributions of this paper are: 1) formulating a weighted cost function that consists of system performance and switching smoothness index, with a tunable parameter to balance the two; 2) providing PLMIs for switching ICC/$\mathcal{H}_\infty$ LPV DOF control design; 3) applying smooth-switching LPV control to vibration suppression of the BWB flexible wing. The simulation results validate that the proposed method is capable of balancing switching smoothness and system performance. Furthermore, the tunable parameter also provides an extra degree of freedom for tuning control gain, which is critical for practical applications.

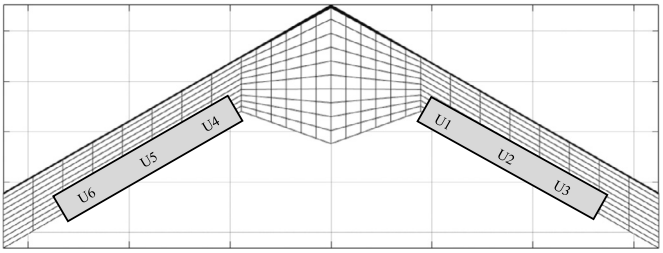

Fig. 1. Schematic layout of BWB airplane configuration.

This paper is organized as follows. Section 2 introduces the LPV modeling of the BWB airplane wing and specifies the associated system performance requirements. Section 3 provides synthesis conditions for smooth-switching LPV control design. Simulation results and associated discussions are provided in Section 4. Finally, conclusions are drawn in Section 5.

2. LPV model of the BWB airplane wing

2.1. LPV modeling

In this section, we consider the LPV modeling of BWB flexible wing, see Fig. 1 for a schematic illustration. Assume that the BWB airplane is flying at a fixed altitude but with varying flight speed. The main body of BWB is gridded into six beam elements and each wing is gridded into four beam elements. The inner three elements at each wing are selected as control surfaces, labeled as U1–U6 in Fig. 1, and wing bending displacements are to be suppressed by activating the control surfaces. In order to modulate the vibrational behaviors of entire airplane wings, a total of 24 bending displacements are selected as system outputs. For example, outputs 1 and 12 are the nodal displacements at the right wing root and right wing tip in Fig. 1.

The LPV modeling procedure can be described as follows: 1) a bundle of LTI full-order models (FOMs) are derived by linearizing nonlinear aero-elastic model at each gridded flight speed [2]; 2) FOMs are then transformed into modal coordinates and all system modes are properly aligned to track mode variations from one flight speed to the next; 3) model-reduction is conducted to keep the most significant modes over the entire gridded flight envelop [1]; 4) linear interpolation over the aligned reduced-order models to attain the affine LPV model. The interpolation of aligned modes is able to capture the variation of system's coupled aerodynamic mode with varying flight speed, which cannot be achieved by direct interpolation of LTI system matrices [1].

In this study, the scheduling parameter is chosen to be the airplane flight speed, and it ranges from 110 to 130 m/s. A bundle of reduced-order LTI models are derived at varying flight speeds and at an increment of 0.5 m/s to capture model variation. Six dominant modes are kept in the reduced-order LTI models, as marked by M1–M6 in Fig. 2. Physical meanings of these modes are summarized in Table 1. Note that all the bending/torsion coupling effects come from the backswept of the wing, and the wing structural rigidity itself has no inherent bending/torsion coupling. The vibration modes stay stable when flight speed is below 115 m/s, and mode M1 becomes unstable beyond 115 m/s as shown in Fig. 2.

The affine LPV model is obtained by linearly interpolating the first and last eigenvalues of each mode. As shown in the close-up view of Fig. 2, the solid line shows the linear interpolation of the eigenvalues, where crosses denote the loci of actual eigenvalues as function of flight speed. As a result, in the interpolated affine LPV model, system damping coefficient is approximated while system

Table 1
Mode description in reduced-order model.

Mode ID	Rigid-body component	Flexible component	Note
M1	Plunging and pitching	First symmetric out-of-plane bending	Bending/torsion coupling
M2	Plunging and pitching	Second symmetric out-of-plane bending	Bending/torsion coupling
M3	Plunging and pitching	First symmetric in-plane bending	Bending/torsion coupling
M4	Roll	Second anti-symmetric out-of-plane bending	Bending/torsion coupling
M5	–	First anti-symmetric in-plane bending	Bending/torsion coupling
M6	–	–	Aerodynamic dominant mode

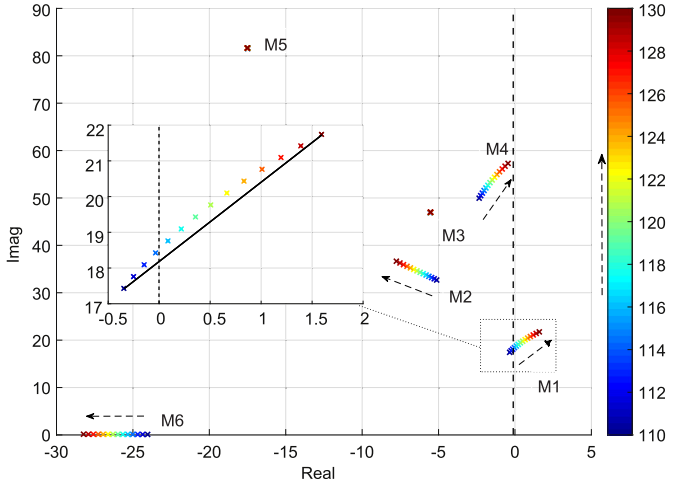

Fig. 2. Root loci of open-loop system with varying flight speed. (For interpretation of the colors in the figure(s), the reader is referred to the web version of this article.)

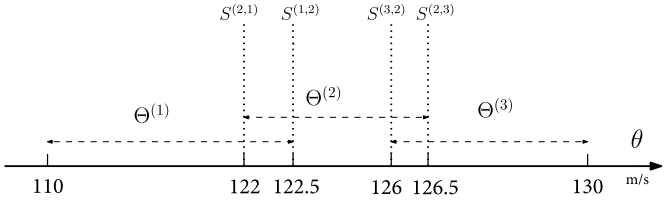

Fig. 3. Three-subregion partition for scheduling parameter.

stability remains unchanged over the entire flight envelope. Similarly, all other system matrices are also obtained by following the same linear interpolation process. The resulted affine LPV model consists of 12 states (6 modes), 6 control inputs (control surfaces deflection angles) and 24 performance outputs (wing bending displacements).

There are two main control design goals. One is to robustly stabilize the closed-loop system under bounded modeling error and the other is to suppress wing bending displacements, excited by the gust disturbance, using control surfaces on the wing. As a result, two independent $\mathcal{H}_\infty$ and $\mathcal{H}_2$ input channels are used along with two independent $\mathcal{H}_\infty$ and $\mathcal{H}_2$ output channels for the system described in Eqn. (1) and Fig. 4, where modeling error is modeled as system disturbance input w_∞ excited by the system output z_∞ through uncertainty Δ and the closed-loop robust stability is achieved by satisfying the desired $\mathcal{H}_\infty$ performance; the gust disturbance is treated as disturbance input w_2 with associated $\mathcal{H}_2$ performance output z_2 to be optimized for suppressing bending displacement z_2 caused by the gust disturbance. In addition, ICC constraints are imposed on control inputs or deflection angles of control surfaces, so that they are hard-constrained to operate within their limits. In order to apply switching LPV control, the switching LPV model is developed by dividing the scheduling parameter range into multiple overlapping subregions, as shown in Fig. 3. In the next subsection, a generic LPV model with $\mathcal{H}_\infty$ and $\mathcal{H}_2$ channels will be considered and the associated system performances defined.

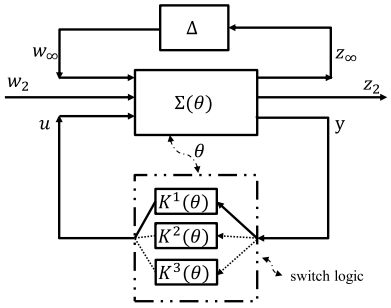

Fig. 4. Switching multi-objective LPV control scheme.

2.2. Affine LPV system with multiple regions

Consider the LPV system $\Sigma(\theta)$ with $\mathcal{H}_\infty$ and $\mathcal{H}_2$ channels,

$$\begin{aligned}
\dot{x}_p(t) &= A\big(\theta(t)\big)x_p(t) + B_1\big(\theta(t)\big)w_\infty(t) + B_2\big(\theta(t)\big)w_2(t) \\
&\quad + B_u\big(\theta(t)\big)u(t) \\
z_\infty(t) &= C_1\big(\theta(t)\big)x_p(t) + D_1\big(\theta(t)\big)w_\infty(t) + D_2\big(\theta(t)\big)u(t) \\
z_2(t) &= C_2\big(\theta(t)\big)x_p(t) \\
y(t) &= C_y\big(\theta(t)\big)x_p(t) + D_y w_\infty(t)
\end{aligned} \tag{1}$$

where $\theta(t)$ denotes the scheduling parameter, $x_p(t)$ the model state, $u(t)$ the control input, and $y(t)$ the measured bending displacements. In the $\mathcal{H}_\infty$ channel, $w_\infty(t)$ denotes the exogenous input, which includes system disturbance, sensor noise, etc., while $z_\infty(t)$ denotes the $\mathcal{H}_\infty$ controlled output. In the $\mathcal{H}_2$ channel, $w_2(t)$ denotes the disturbance input, such as gust disturbance, and $z_2(t)$ the $\mathcal{H}_2$ controlled output or wing bending displacements. All system matrices are in affine parameter-dependent form; for example,

$$A(\theta(t)) = A_0 + \sum_{i=1}^{q} A_i\theta_i(t), \quad \theta = [\theta_1, \theta_2, ..., \theta_q], \tag{2}$$

where q is the dimension of scheduling parameter. The scheduling parameter is assumed to be measurable in real-time, and its admissible set is formed by its magnitude and rate bounds as Eqn. (3). In this study, the flight speed measurement is available with the current speedometer, and flight speed bounds and acceleration bounds are determined by flight envelop of interest. Note that measurement uncertainty is not considered in this paper.

$$\theta \in \Theta = \left\{\underline{\theta}_i \le \theta_i(t) \le \bar{\theta}_i, -\nu_{\theta i} \le \dot{\theta}_i(t) \le \nu_{\theta i}\,;\, i = 1, ..., q\right\}. \tag{3}$$

The size of scheduling parameter region would influence the achievable system performance, thus smooth-switching LPV control design is performed by dividing single parameter region into a few small subregions for improving achievable system performance. The scheduling parameter region is divided into multiple subregions, with an overlapping region between any two adjacent subregions. The jth subregion is denoted by $\Theta^{(j)}$ ($j \in N_J = [1, 2, \ldots, J]$), and switching surface from $\Theta^{(i)}$ to $\Theta^{(j)}$ ($i, j \in N_J$, $i \neq j$) is denoted by $S^{(i,j)}$.

In the derived LPV aeroelastic model, since only the flight speed is considered the scheduling parameter, hence $q = 1$. The partition of flight speed envelope shown in Fig. 3 indicates that $N_J = 3$. A family of gain-scheduling LPV DOF controllers are designed, and adjacent controllers are switched according to hysteresis switching logic [6]. The switching LPV control scheme is illustrated in Fig. 4. When θ crosses the switching surface $S^{(i,j)}$, ith subregion controller $K^i(\theta)$ is switched to jth subregion controller $K^j(\theta)$, and when θ crosses the switching surface $S^{(j,i)}$, then $K^j(\theta)$ is switched back to $K^i(\theta)$. The proposed DOF controller $K^j(\theta)$ for jth subregion is given by

$$K^j(\theta): \begin{cases} \dot{x}_K = A_K^j(\theta)x_K + B_K^j(\theta)y \\ u = C_K^j(\theta)x_K \end{cases} \tag{4}$$

Note that there is no direct feed-through term in u, because a strictly proper DOF controller is needed so that it leads to a finite $\mathcal{H}_2$ norm for transfer functions $T_{z_2 w_2}$ and $T_{u w_2}$. The closed-loop LPV system has the following state-space realization with $x_{cl}^T = [x_p^T, x_K^T]$ on the jth subregion:

$$\left[\begin{array}{c|cc} A_{cl}^j & B_{cl,\infty}^j & B_{cl,2}^j \\ \hline C_{cl,\infty}^j & D_{cl,\infty}^j & \mathbf{0} \\ C_{cl,2}^j & \mathbf{0} & \mathbf{0} \end{array}\right] = \left[\begin{array}{cc|cc} A & B_u C_K^j & B_1 & B_2 \\ B_K^j C_y & A_K^j & B_K^j D_y & \mathbf{0} \\ \hline C_1 & D_2 C_K^j & D_1 & \mathbf{0} \\ C_2 & \mathbf{0} & \mathbf{0} & \mathbf{0} \end{array}\right] \tag{5}$$

For simplicity, the functional dependency on scheduling parameter θ will be omitted hereafter.

2.3. Performance specifications and some useful lemmas

2.3.1. $\mathcal{H}_\infty$ performance ($\mathcal{L}_2$–$\mathcal{L}_2$ gain)

The $\mathcal{H}_\infty$ channel is designated to guarantee the robust stability of closed-loop system in the presence of modeling errors. Let $T_\infty(\theta, s) := T_{z_\infty w_\infty}(\theta, s)$ denotes the parameter-dependent transfer function from $w_\infty(t)$ to $z_\infty(t)$ and $||T_\infty||_\infty$ the $\mathcal{H}_\infty$ norm of T_∞. Then, the $\mathcal{H}_\infty$ performance for the pair $(w_\infty(t), z_\infty(t))$ is defined as

$$||T_\infty||_\infty = \sup_{\theta\in\Theta^{(j)}, j\in N_J} \sup_{z_\infty, w_\infty\in\mathcal{L}_2, w_\infty\neq 0} \frac{||z_\infty(t)||_2}{||w_\infty(t)||_2}. \tag{6}$$

Lemma 1. *[8] Suppose there exists a family of parameter dependent positive-definite matrices $P_\infty^j(\theta)$, such that (7) holds for any subregion $\Theta^{(j)}$, and (8) holds for any adjacent $\Theta^{(i)}$ and $\Theta^{(j)}$ $(i, j \in N_J, i \neq j)$, then with the switching LPV controller (4) and hysteresis switching logic, the closed-loop system (5) is exponentially stable and $||z_\infty||_2 < \gamma||w_\infty||_2$ is achieved with given robustness level $\gamma > 0$ for all admissible trajectories $\theta(t) \in \Theta$.*

$$\begin{bmatrix} -\dot{P}_\infty^j + A_{cl}^j P_\infty^j + (*) & * & B_{cl}^j \\ C_{cl,\infty}^j P_\infty^j & -\gamma I & D_{cl,\infty}^j \\ * & * & -\gamma I \end{bmatrix} < 0, \tag{7}$$

$$P_\infty^j(\theta) \le P_\infty^i(\theta), \quad \theta \in S^{(i,j)}. \tag{8}$$

2.3.2. $\mathcal{H}_2$ performance

The $\mathcal{H}_2$ performance, defined from $w_2(t)$ to $z_2(t)$, is utilized to assess the closed-loop performance against external disturbance. Let $T_2(\theta, s) := T_{z_2 w_2}(\theta, s)$ be the parameter-dependent transfer function from $w_2(t)$ to $z_2(t)$, and if the subregion system A_{cl}^j is stable, the $\mathcal{H}_2$ norm is defined by the worst-case $\mathcal{H}_2$ performance on the subregion $\Theta^{(j)}$ [12]

$$||T_2||_2^2 = \sup_{\theta\in\Theta^{(j)}, j\in N_J} trace(C_{cl,2}^j(\theta)\bar{P}_2^j(\theta)C_{cl,2}^j(\theta)^T) \tag{9}$$

where $\bar{P}_2^j$ solves the differential Riccati equation, $\dot{\bar{P}}_2^j = A_{cl}^j\bar{P}_2^j + \bar{P}_2^j(A_{cl}^j)^T + B_{cl}^j(B_{cl}^j)^T$, with zero initial condition. Note that the following relationship holds,

$$\sup_{w_2\in\mathcal{L}_2, w_2\neq 0} \frac{||z_2(t)||_\infty}{||w_2(t)||_2} \le ||T_2||_2,$$

where the equality holds when the dimension of z_2 is one. The $\mathcal{H}_2$ norm of a deterministic system is denoted by the square summation of $\mathcal{L}_2$ to $\mathcal{L}_\infty$ gains of individual channels from exogenous disturbance inputs to system outputs. In this study, the $\mathcal{H}_2$ norm is a measure of bending displacements ($\mathcal{L}_\infty$ norm) due to energy bounded ($\mathcal{L}_2$ norm) gust disturbance. Alternatively, the $\mathcal{H}_2$ norm can be interpreted as deterministic covariance of system outputs in terms of time correlation [13]. Optimizing the $\mathcal{H}_2$ performance means suppressing closed-loop output responses against $\mathcal{L}_2$ disturbance. We have the following lemma.

Lemma 2. *[14] For a stable A_{cl}^j, if there exist a parameter dependent positive-definite matrix $P_2^j(\theta)$ and a constant matrix W, such that,*

$$\begin{bmatrix} -\dot{P}_2^j + A_{cl}^j P_2^j + (*) & B_{cl}^j \\ * & -I \end{bmatrix} < 0, \tag{10}$$

$$\begin{bmatrix} W & C_{cl,2}^j P_2^j \\ * & P_2^j \end{bmatrix} > 0, \tag{11}$$

then, the $\mathcal{H}_2$ norm of the closed-loop system on any jth subregion is bounded by trace(W), i.e.

$$trace(C_{cl,2}^j(\theta)P_2^j(\theta)C_{cl,2}^j(\theta)^T) < trace(W). \tag{12}$$

The above lemma shows that the $\mathcal{H}_2$ norm at $\Theta^{(j)}$ subregion is bounded by *trace*(W), hence the optimal solution can be achieved by minimizing the upper bound *trace*(W).

2.3.3. Input Covariance Constraint (ICC) [3]

The control input is given as

$$u(t) = C_u^j x_{cl} = \begin{bmatrix} 0 & C_K^j \end{bmatrix} \begin{bmatrix} x_p \\ x_K \end{bmatrix}.$$

Hence, the variance of kth control input of jth controller is bounded as

$$cov(u_k(\theta(t))) \le \sup_{\theta\in\Theta^{(j)}, j\in N_J} e_k C_u^j \bar{P}_2^j (C_u^j)^T e_k^T = U_k,$$

where e_k is a selection row vector such that $e_k C_u^j$ equals to the kth row of matrix C_u^j, and $\bar{P}_2^j$ is given by (9). The following lemma provides hard constraint on variance of the kth control input for any $\theta \in \Theta^{(j)}$.

Lemma 3. *[3] The ICC condition of the kth control input of the jth controller*

$$U_k = e_k C_u \bar{P}_2^j C_u^T e_k^T < e_k C_u P_2^j C_u^T e_k^T < \bar{U}_k \tag{13}$$

is equivalent to

$$\begin{bmatrix} \bar{U}_k & e_k C_u^j P_2^j \\ * & P_2^j \end{bmatrix} > 0, \quad k = 1, 2, \cdots, n_u, \tag{14}$$

where n_u is the number of control inputs.

3. Smooth switching LPV DOF controller design

The following theorem provides the controller synthesis conditions for simultaneous design of smooth switching LPV DOF controller. The cost function (15) is a linear combination of two convex functions of output performance $trace(W)$ and smoothness index I_{sm} that is a function of controller variables. The tunable parameter ϵ is used to balance the output performance and smoothness of controller parameters over switching surfaces. A line search for ϵ is recommended in order to find the optimal trade-off relationship. The main result of this paper is contained in the following theorem.

Theorem 1. *For the LPV system (1) with divided subregions, a family of gain-scheduling DOF controllers (4) minimize the ϵ-balanced cost function*

$$\min_{\hat{A}_K^j,\hat{B}_K^j,\hat{C}_K^j X^j,Y^j} \quad \epsilon * trace(W) + I_{sm} \tag{15}$$

subject to the ICC constraint (13) and $\mathcal{H}_\infty$ constraints (7) and (8), if there exist a family of parameter-dependent symmetric matrices X^j and Y^j, and a family of parameter-dependent controller variables $\hat{A}_K^j$, $\hat{B}_K^j$, and $\hat{C}_K^j$ ($j \in N_J$), such that the PLMIs (17)–(21) hold for a given robustness level $\gamma > 0$ and all admissible $\theta \in \Theta$ with one of the two conditions in (22) satisfied on the switching surfaces for $\epsilon > 0$. Furthermore, the smoothness index I_{sm} is defined as

$$I_{sm} = \sum_{i,j,i\neq j} \begin{pmatrix} ||\hat{A}_K^i - \hat{A}_K^j||_2 + ||\hat{B}_K^i - \hat{B}_K^j||_2 \\ +||\hat{C}_K^i - \hat{C}_K^j||_2 + ||Y^i - Y^j||_2 \\ +||X^i - X^j||_2 \end{pmatrix} |_{\theta\in S^{(i,j)}}. \tag{16}$$

$$\begin{bmatrix} M_{11} & * & * & * \\ A^T + \hat{A}_K^j & M_{22} & * & * \\ B_1^T & M_{32} & -\gamma I & * \\ C_1 X^j + D_2 \hat{C}_K^j & C_1 & D_1 & -\gamma I \end{bmatrix} < 0 \tag{17}$$

where

$$M_{11} = AX^j + B_u \hat{C}_K^j + (*) - \dot{X}^j,$$
$$M_{22} = Y^j A + \hat{B}_K^j C_y + (*) + \dot{Y}^j,$$
$$M_{32} = \left(Y^j B_1 + \hat{B}_K^j D_y\right)^T.$$

$$\begin{bmatrix} X^j & I \\ I & Y^j \end{bmatrix} > 0 \tag{18}$$

$$\begin{bmatrix} M_{11} & * & * \\ A^T + \hat{A}_K^j & M_{22} & * \\ B_2^T & (Y^j B_2 + \hat{B}_K^j D_y)^T & -I \end{bmatrix} < 0 \tag{19}$$

$$\begin{bmatrix} W & C_1 X^j + D_2 \hat{C}_K^j & C_1 \\ * & X^j & I \\ * & I & Y^j \end{bmatrix} > 0 \tag{20}$$

$$\begin{bmatrix} \bar{U}_k & e_k \hat{C}_K^j & 0 \\ * & X^j & I \\ * & I & Y^j \end{bmatrix} > 0, \quad k = 1, 2, \cdots, n_u. \tag{21}$$

$$\begin{cases} Y^i \geq Y^j \\ X^i - (Y^i)^{-1} \leq X^j - (Y^j)^{-1} \end{cases} \text{ or } \begin{cases} X^i \leq X^j \\ Y^i - (X^i)^{-1} \geq Y^j - (X^j)^{-1} \end{cases} \tag{22}$$

Proof. This theorem is proved based on Lemmas 1–3. To convexify control strategy with $\mathcal{H}_2$ and $\mathcal{H}_\infty$ channels, let $P_2^j = P_\infty^j$ for the jth subregion. Suppose the Lyapunov matrix P^j can be partitioned as

$$P^j = \begin{bmatrix} Y^j & N^j \\ (N^j)^T & \star \end{bmatrix}, \quad (P^j)^{-1} = \begin{bmatrix} X^j & M^j \\ (M^j)^T & \star \end{bmatrix} \tag{23}$$

Furthermore, define the congruence matrices $\Pi_1^j = \begin{bmatrix} X^j & I \\ (M^j)^T & 0 \end{bmatrix}$, $\Pi_2^j = \begin{bmatrix} I & Y^j \\ 0 & (N^j)^T \end{bmatrix}$, such that $P^j \Pi_1^j = \Pi_2^j$. Introduce the change of controller variables as

$$\begin{aligned} \hat{A}_K^j &= N^j A_K^j (M^j)^T + N^j B_K^j C_y X^j + Y^j B_2 C_K^j (M^j)^T + Y^j A X^j \\ \hat{B}_K^j &= N^j B_K^j \\ \hat{C}_K^j &= C_K^j (M^j)^T \end{aligned} \tag{24}$$

For the $\mathcal{H}_\infty$ performance channel, the PLMIs (17) can be easily obtained by following the procedures in [8]. For the $\mathcal{H}_2$ performance channel, define the congruence matrix $T_2 = diag(\Pi_2^j, I)$. Pre- and post-multiply (10) by T_2^T and T_2 to obtain,

$$T_2^T \begin{bmatrix} -\dot{P}^j + A_{cl}^j P^j + (*) & B_{cl}^j \\ * & -I \end{bmatrix} T_2 < 0, \tag{25}$$

which yields (19). Define $T_3 = diag(I, \Pi_2)$, and pre- and post-multiply (11) by T_1^T and T_1, we obtain

$$\begin{bmatrix} I & \\ & \Pi_2^T \end{bmatrix} \begin{bmatrix} W & C_{cl,2}^j P^j \\ * & P^j \end{bmatrix} \begin{bmatrix} I & \\ & \Pi_2 \end{bmatrix} > 0, \tag{26}$$

which yields (20). For the ICC condition, pre- and post-multiplying T_3^T and T_3 to (14) yields

$$\begin{bmatrix} I & \\ & \Pi_2^T \end{bmatrix} \begin{bmatrix} \bar{U}_k & e_k C_u^j P_2^j \\ * & P_2^j \end{bmatrix} \begin{bmatrix} I & \\ & \Pi_2 \end{bmatrix} > 0, \tag{27}$$

which gives (21). □

Remark 1. The usage of $P_2^j = P_\infty^j$ convexifies formulated PLMIs and makes optimization problem numerically tractable, and as a result, this condition will impose conservatism into the optimization result. [15] The PLMIs formulated in Theorem 1 renders an optimization problem of infinite dimensions with indetermined variables. To numerically tackle this problem, affine variable structure is assumed, for example, $\hat{A}_K^j(\theta)$ is expressed as $\hat{A}_K^j(\theta) = \hat{A}_{K0}^j + \sum_{i=1}^{q} \hat{A}_{Ki}^j \theta_i$. Coefficient check in multi-simplex domain by Polya theorem [16] is adopted to attain a finite set of LMIs. Other relaxation methods, such as the enforcing multi-convexity method [17] and sum-of-square matrices [18] can also be used to solve the problem. The operation of PLMIs and optimization problem are solved by using the parser ROLMIP [19], YALMIP [20] jointly with optimization algorithm SeDuMi [21].

Remark 2 *(Controller reconstruction).* If controller variables are obtained by minimizing the ϵ-*balanced* cost function subject to formulated PLMIs, the gain-scheduling DOF controller can be constructed by first solving the factorization problem $I - Y^j X^j = N^j (M^j)^T$ for N^j and M^j, and then computing A_K^j, B_K^j, and C_K^j from the following equations,

$$\begin{cases} A_K^j = \left(N^j\right)^{-1} \left[\hat{A}_K^j - Y^j \dot{X}^j - N^j \left(\dot{M}^j\right)^T - Y^j A X^j - \hat{B}_K^j C_y X^j \right. \\ \qquad \left. -Y^j B_2 \hat{C}_K^j \right] \left(M^j\right)^{-T} \\ B_K^j = N^{-1} \hat{B}_K^j \\ C_K^j = \hat{C}_K \left(M^j\right)^{-T} \end{cases} \tag{28}$$

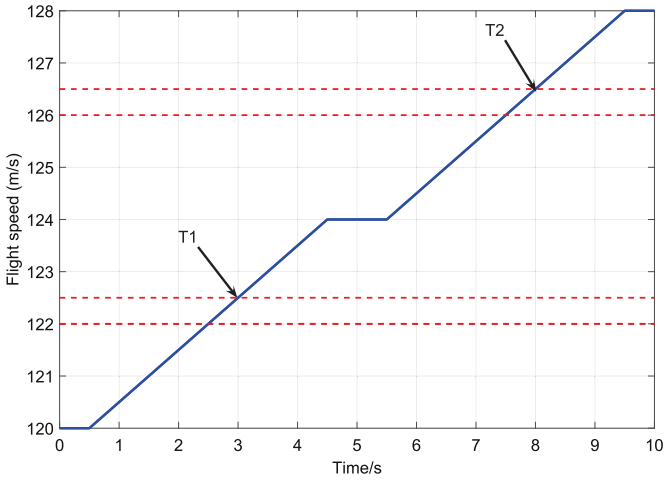

Fig. 5. Scheduling parameter with switching events.

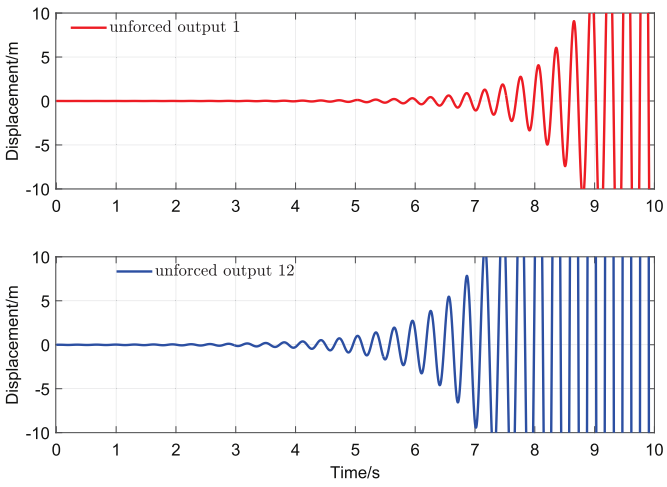

Fig. 6. Unforced bending displacements at wing root (upper) and wing tip (lower).

Remark 3 *(Practical validity).* In order to remove the $\dot{\theta}$ dependency introduced by $\dot{X}^j$ and $\dot{Y}^j$, the practical validity approach presented in [22] is applied. Since factorization does not affect the existence of a controller, setting either X^j or Y^j to be a constant matrix eliminates the derivative terms. For example, we may set $X(\theta) = X_0$ and $N = I$ for all $\theta \in \Theta^{(j)}$, then $Y^j = Y^j(\theta)$ and $(M^j)^T = (I - Y^j(\theta)X_0)$. As a result, the reconstructed controller variables can be simplified as

$$\begin{cases} A_K^j = (N^j)^{-1}\left[\hat{A}_K^j - Y^j A X^j - \hat{B}_K^j C_y X^j - Y^j B_2 \hat{C}_K^j\right](M^j)^{-T} \\ B_K = N^{-1}\hat{B}_K^j \\ C_K = \hat{C}_K (M^j)^{-T} \end{cases} \tag{29}$$

Note that the switching stability condition (22) is non-convex and is convexified by the selection of frozen $X(\theta)$ and $Y^i(\theta) \geq Y^j(\theta),\ \theta \in S^{(i,j)}$. Therefore, matrix-valued coefficient of affine controller variables $(\hat{A}_{Ki}^j, \hat{B}_{Ki}^j, \hat{C}_{Ki}^j, Y_i^j, X_0)$, $i = 0, 1, \cdots, q$, are searched to optimize the cost function with the tuning parameter ϵ.

4. Simulation results and discussion

The scenario that a BWB airplane experiences a sharp gust disturbance is considered in this study. The gust disturbance is assumed to induce a constant shift angle w_2 on all control surfaces for $t \in [0, 9]$ second, and we assume that $w_2 = 0.005$ rad $\approx 0.28°$. As shown in Fig. 5, two switching events happen at $t = T_1 = 3$ s and $t = T_2 = 8$ s. Therefore, within the time interval of $[0, 10]$ second, the scheduling parameter is bounded by 110 m/s $\leq \theta \leq$ 130 m/s, and its rate bounded by -1 m/s^2 $\leq \dot{\theta} \leq 1$ m/s^2. Note that when the open-loop system is subject to gust disturbance, bending displacements are unstable, as shown in Fig. 6. A family of smooth-switching mixed $ICC/\mathcal{H}_\infty$ LPV DOF controllers are to be designed using Theorem 1 for stability as well as achieving a balanced $\mathcal{H}_2$ performance and switching smoothness, with guaranteed $\mathcal{H}_\infty$ robust performance (at $\gamma = 10$).

The trade-off relationship is explored by line search of weighting coefficients ϵ under different ICC constraints: $\bar{U}_1 = 8$, $\bar{U}_2 = 12$ and $\bar{U}_3 = 20$. As shown in Fig. 7, the switching smoothness index can be reduced by decreasing weighting coefficient ϵ, which results in an increased in $\mathcal{H}_2$ performance index $trace(W)$ or degraded $\mathcal{H}_2$ performance. This illustrates that system performance is sacrificed in order to enforce switching smoothness. Especially,

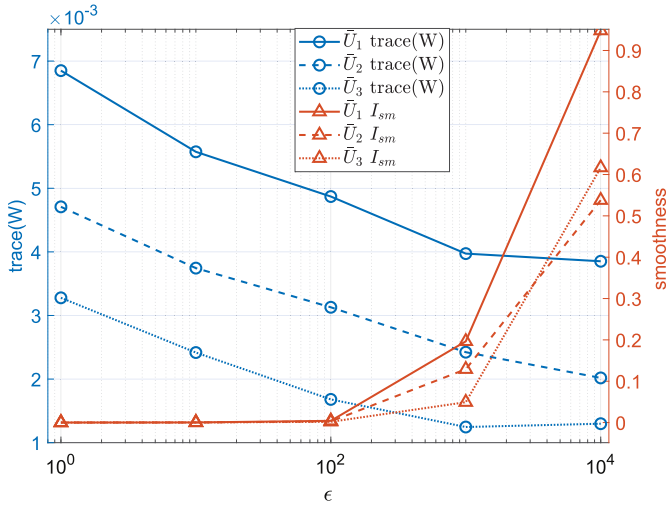

Fig. 7. Trade-off between $trace(W)$ and smoothness index I_{sm}.

when $\epsilon < 10^2$, the system performance index increases significantly for all three ICC constraints, indicating that system performance is degrading much drastically in order to achieve smoother responses. Thus, an optimal weighting coefficient is chosen to be $\epsilon = 10^2$ to attain smooth switching with acceptable system performance. To demonstrate that this balanced result is attainable, extensive simulations are conducted by considering three different controllers: 1) non-switching LPV controller, 2) un-smooth switching LPV controller, and 3) the proposed smooth-switching LPV controller. And these controllers are applied to the BWB flexible wing for vibration suppression.

Figs. 8 and 9 show the bending displacement at wing root (output 1) and wing tip (output 12), respectively, where as Figs. 10–15 show the control allocation of deflection angles of six flaps according to three different control strategies.

In upper sub-figure of Fig. 9, smooth (blue) and un-smooth (red) responses of bending displacement at wing root are shown. At switching event $T_1 = 3$ s, controller 1 is switched to controller 2 and the sudden changes of un-smooth controllers cause abrupt jumps for all three different ICC conditions. On the other hand, the smooth-switching LPV controllers enforce smooth output responses, with slightly increased bending displacement as a minor penalty on system performance. Similar behaviors can be observed at the switching event $T_2 = 8$ s. Another trade-off relationship can be observed from output responses. Different ICC constraints will

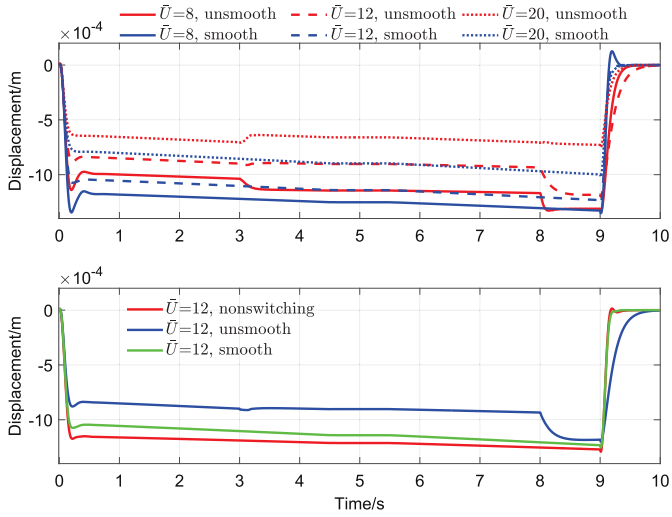

Fig. 8. Upper: comparison at wing root with smooth/un-smooth switching controller; Lower: comparison at wing root with three control methods.

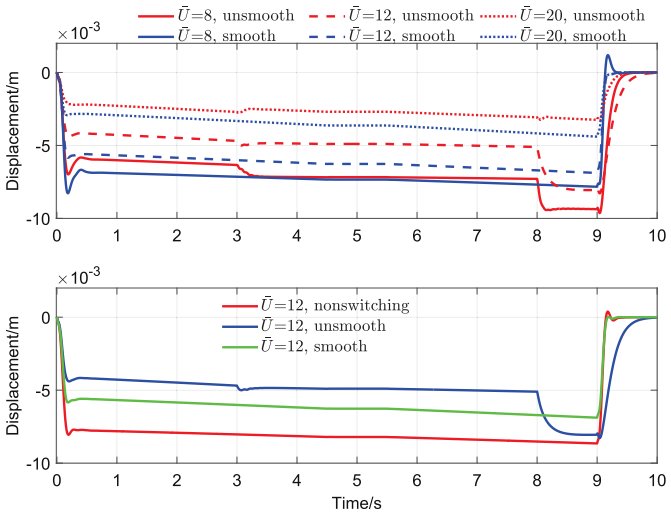

Fig. 9. Upper: comparison at wing tip with smooth/un-smooth switching controller; Lower: comparison at wing tip with three control methods.

influence the optimal achievable system performance. With larger control input, the bending displacements can be suppressed even further, however, when $\bar{U} > 12$, much more control effort will be consumed to further improve system performance, as seen from control responses in Figs. 10–15. Therefore, the hard constraint on control input is chosen at $\bar{U} = 12$, in order to achieve acceptable performance and energy saving.

The lower sub-figure of Fig. 9 shows the comparison of wing tip responses with three different controllers. As shown, all three control methods are able to stabilize and suppress bending displacements for the entire flight speed envelope. It can be further observed that both smooth and un-smooth switching LPV controllers produce smaller magnitude of bending displacements than the non-switching LPV controller, and this is achieved by relaxing the PLMI conservativeness and enforcing the optimal performance on each subregion. However, un-smooth switching LPV leads to undesirable jump on the bending displacement at wing tip, which is effectively smoothened by the proposed smooth-switching LPV controller.

The responses of control input also demonstrate the effectiveness of proposed control method. In the upper sub-figures of Figs. 10–15, un-smooth control design results in control inputs exhibiting sharp jump at the switching events, but theses jumps are effectively removed by the proposed smooth-switching LPV controllers. Especially at switching event $T_2 = 8$ s, un-smooth switching controller commands the control surfaces to deflect in opposite directions within very short time, which imposes a severe capacity burden on the actuator. Smooth-switching controller, on the other hand, allocates the deflection angles of control surfaces with smooth control commands when switching occurs. In the lower sub-figures, control commands of three control methods are compared. Unlike switching LPV control, non-switching LPV control results in a conservative control input of very small magnitude; due to the conservativeness introduced in PLMIs. Un-smooth switching LPV control is able to relax conservativeness and assign slightly larger control energy, leading to improved vibration suppression of bending displacements. However, by minimizing control gain differences in optimization cost function, smooth-switching LPV control can result in much smoother responses with minor degradation on system performance, which is still better than the performance of the un-smooth switching LPV control.

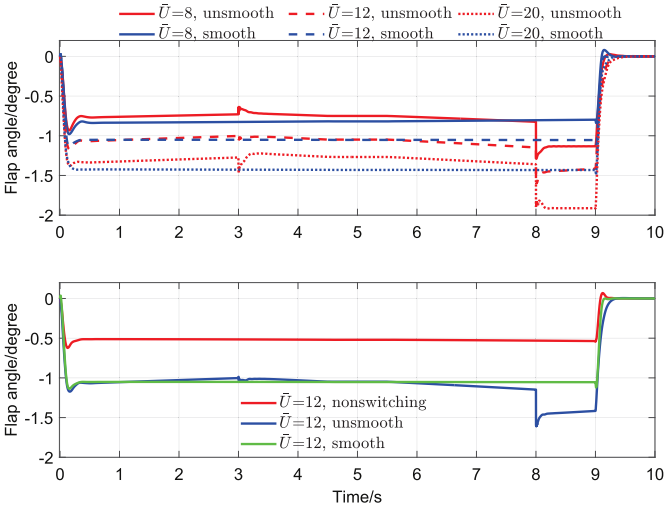

Fig. 10. Upper: control 1 responses comparison with smooth/un-smooth switching controller; Lower: control 1 responses comparison with three control methods.

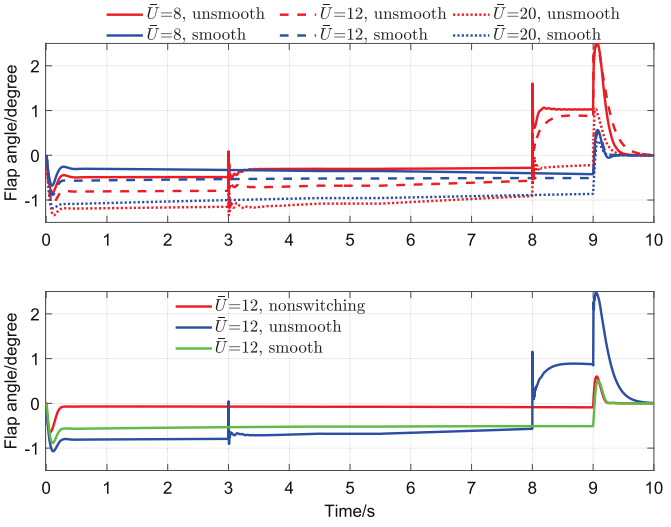

Fig. 11. Upper: control 2 responses comparison with smooth/un-smooth switching controller; Lower: control 2 responses comparison with three control methods.

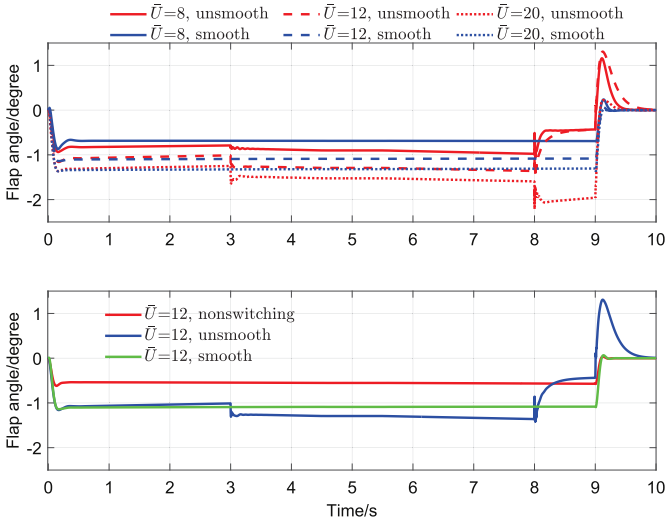

Fig. 12. Upper: control 3 responses comparison with smooth/un-smooth switching controller; Lower: control 3 responses comparison with three control methods.

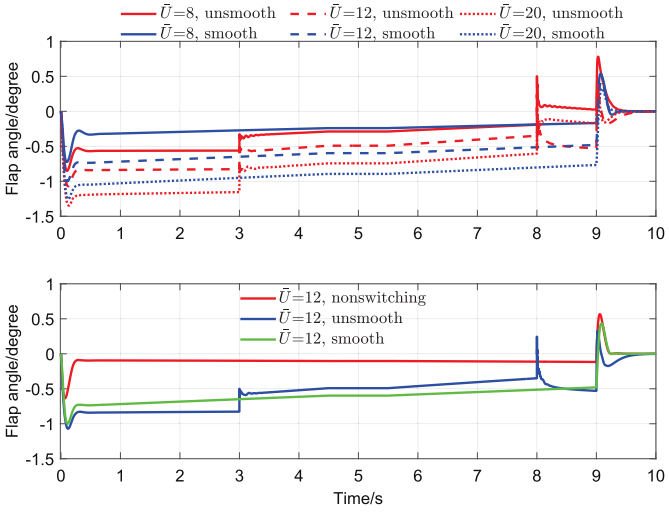

Fig. 13. Upper: control 4 responses comparison with smooth/un-smooth switching controller; Lower: control 4 responses comparison with three control methods.

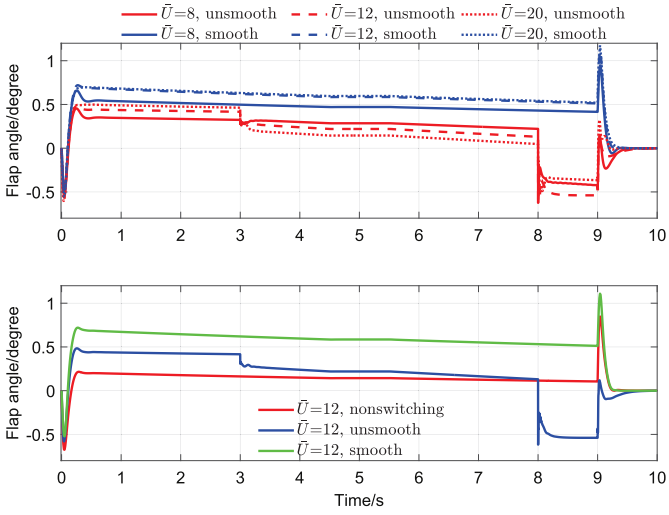

Fig. 14. Upper: control 5 responses comparison with smooth/un-smooth switching controller; Lower: control 5 responses comparison with three control methods.

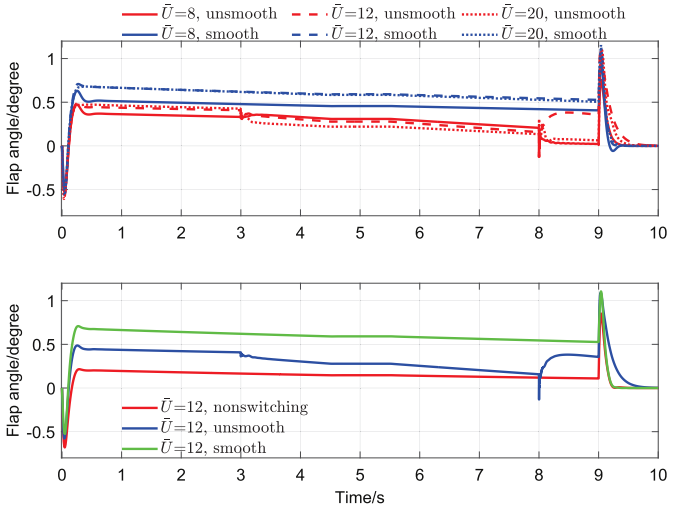

Fig. 15. Upper: control 6 responses comparison with smooth/un-smooth switching controller; Lower: control 6 responses comparison with three control methods.

5. Conclusion

This paper presents a simultaneous control design approach for smooth-switching $ICC/\mathcal{H}_\infty$ dynamic output-feedback LPV controller and its application to vibration suppression of a BWB flexible airplane wing. Both innovative smoothness and system performance indexes were incorporated in the cost function and weighted by a tunable coefficient, leading to an optimal design trade-off between the best achievable $\mathcal{H}_2$ performance and switching smoothness. By this way, the control design method was formulated into a numerically tractable problem, even though certain conservatism was introduced during the convexification and relaxation process. Simulation results showed that the proposed design method is able to significantly reduce the sharp jumps in system controls and responses during switching events. Moreover, the proposed tunable weighting coefficient provides trade-off between system performance and smoothness of response, and the ICC constraints on control inputs can also be used to tune the achievable performance. These offer great advantages in practical implementation. The proposed method is based on prior selected subregion divisions that may not be an optimal choice. The systematic and efficient approach to determine the optimal subregion division is a potential research direction.

Conflict of interest statement

There is no conflict of interest.

Acknowledgements

This research is supported by NASA ARMD Convergent Aeronautics Solutions (CAS) Project.

References

[1] A.K. Al-Jiboory, G.G. Zhu, S.S.-M. Swei, W. Su, N.T. Nguyen, LPV modeling of a flexible wing aircraft using adaptive model gridding and alignment methods, Aerosp. Sci. Technol. 66 (2017) 92–102.
[2] W. Su, C.E. Cesnik, Nonlinear aeroelasticity of a very flexible blended-wing-body aircraft, J. Aircr. 47 (5) (2010) 1539–1553.
[3] A.K. Al-Jiboory, A. White, S. Zhang, G.G. Zhu, J. Choi, Linear matrix inequalities approach to input covariance constraint control with application to electronic throttle, J. Dyn. Syst. Meas. Control 137 (9) (2015) 091010.
[4] T. He, A.K. Al-Jiboory, G.G. Zhu, S.S.-M. Swei, W. Su, Guaranteed $\mathcal{H}_\infty$ performance LPV ICC control with application to blended-wing-body model, in: 2018 AIAA/ASCE/AHS/ASC Structures, Structural Dynamics, and Materials Conference, Kissimmee, 2018.

[5] T. He, A.K. Al-Jiboory, G.G. Zhu, S.S.-M. Swei, W. Su, Application of ICC LPV control to a blended-wing-body airplane with guaranteed $\mathcal{H}_\infty$ performance, Aerosp. Sci. Technol. 81 (2018) 88–98, https://doi.org/10.1016/j.ast.2018.07.046.
[6] B. Lu, F. Wu, Switching LPV control designs using multiple parameter-dependent Lyapunov functions, Automatica 40 (11) (2004) 1973–1980.
[7] B. Lu, F. Wu, S. Kim, Switching LPV control of an F-16 aircraft via controller state reset, IEEE Trans. Control Syst. Technol. 14 (2) (2006) 267–277.
[8] P. Zhao, R. Nagamune, Switching LPV controller design under uncertain scheduling parameters, Automatica 76 (2017) 243–250.
[9] T. He, A.K. Al-Jiboory, S.S.-M. Swei, G.G. Zhu, Switching state-feedback LPV control with uncertain scheduling parameters, in: American Control Conference, Seattle, 2017, pp. 2381–2386.
[10] P. Chen, The design of smooth switching control with application to V/STOL aircraft dynamics under input and output constraints, Asian J. Control 14 (2) (2012) 439–453.
[11] M. Hanifzadegan, R. Nagamune, Smooth switching LPV controller design for LPV systems, Automatica 50 (5) (2014) 1481–1488.
[12] C.W. Scherer, Mixed $\mathcal{H}_2/\mathcal{H}_\infty$ control for time-varying and linear parametrically-varying systems, Int. J. Robust Nonlinear Control 6 (9–10) (1996) 929–952.
[13] R.E. Skelton, T. Iwasaki, K. Grigoriadis, A Unified Algebraic Approach to Linear Control Design, Taylor & Francis Ltd., London, UK, 1998.
[14] C.E. de Souza, A. Trofino, Gain-scheduled $\mathcal{H}_2$ controller synthesis for linear parameter varying systems via parameter-dependent Lyapunov functions, Int. J. Robust Nonlinear Control 16 (5) (2006) 243–257.
[15] C. Scherer, P. Gahinet, M. Chilali, Multiobjective output-feedback control via LMI optimization, IEEE Trans. Autom. Control 42 (7) (1997) 896–911, https://doi.org/10.1109/9.599969.
[16] R.C.L.F. Oliveira, P. Bliman, P.L.D. Peres, Robust LMIs with parameters in multi-simplex: existence of solutions and applications, in: 47th IEEE Conference on Decision and Control, 2008, pp. 2226–2231.
[17] P. Gahinet, P. Apkarian, M. Chilali, Affine parameter-dependent Lyapunov functions and real parametric uncertainty, IEEE Trans. Autom. Control 41 (3) (1996) 436–442.
[18] C.W. Scherer, C.W.J. Hol, Matrix sum-of-squares relaxations for robust semi-definite programs, Math. Program. 107 (1) (2006) 189–211, https://doi.org/10.1007/s10107-005-0684-2.
[19] C.M. Agulhari, R.C.L.F. de Oliveira, P.L.D. Peres, Robust LMI parser: a computational package to construct LMI conditions for uncertain systems, in: XIX Brazilian Conference on Automation, CBA 2012, Campina Grande, PB, Brazil, 2012, pp. 2298–2305.
[20] J. Löfberg, YALMIP: a toolbox for modeling and optimization in MATLAB, in: Proceedings of the CACSD Conference, Taipei, Taiwan, 2004, pp. 284–289.
[21] J. Sturm, Using SeDuMi 1.02, a MATLAB toolbox for optimization over symmetric cones, Optim. Methods Softw. 11 (1) (1999) 625–653.
[22] P. Apkarian, R.J. Adams, Advanced gain-scheduling techniques for uncertain systems, IEEE Trans. Control Syst. Technol. 6 (1) (1998) 21–32.